



Nanoceria supported palladium(0) nanoparticles: Superb catalyst in dehydrogenation of formic acid at room temperature



Serdar Akbayrak^a, Yalçın Tonbul^b, Saim Özkar^{a,*}

^a Department of Chemistry, Middle East Technical University, 06800 Ankara, Turkey

^b Ziya Gökalp Faculty of Education, Dicle University, 21280 Diyarbakır, Turkey

ARTICLE INFO

Article history:

Received 25 September 2016

Received in revised form 15 January 2017

Accepted 23 January 2017

Available online 24 January 2017

Keywords:

Ceria

Palladium nanoparticles

Formic acid

Hydrogen generation

Dehydrogenation

ABSTRACT

Highly efficient dehydrogenation of formic acid (FA) at room temperature was achieved using palladium(0) nanoparticles supported on nanoceria (Pd^0/CeO_2) as catalysts. Pd^0/CeO_2 was prepared by impregnation of palladium(II) ions on the surface of ceria followed by their reduction with sodium borohydride in aqueous solution at room temperature. Pd^0/CeO_2 was isolated from the reaction solution by centrifugation and characterized by a combination of advanced analytical techniques. The catalytic activity of Pd^0/CeO_2 samples with various Pd loading in the range 1.0–5.0% wt was tested in dehydrogenation of formic acid plus sodium formate with a molar ratio of FA/SF = 1/9. Pd^0/CeO_2 with Pd loading of 2.27% wt shows superb catalytic activity in dehydrogenation of FA with a turnover frequency (TOF) value of 1400 h^{-1} at $25.0 \pm 0.1^\circ\text{C}$. The superb catalytic activity of Pd^0/CeO_2 is ascribed to the reducible nature of ceria during the decomposition of FA ($\text{HCO}_2\text{H} \rightarrow \text{CO}_2 + \text{H}_2$). The kinetic data, obtained by measuring the volume of pure H_2 gas, could be converted to the change in concentration of FA by considering the equilibrium between the formate ion and formic acid ($\text{HCO}_2\text{H} \rightleftharpoons \text{HCOO}^- + \text{H}_3\text{O}^+$). The FA concentration versus time data fit to the first order kinetics with respect to the FA concentration.

© 2017 Elsevier B.V. All rights reserved.

1. Introduction

Formic acid (HCOOH , FA), a major product of biomass processing, is a promising hydrogen carrier due to its high H_2 content (4.4%), nontoxicity and easy recharging ability [1,2]. FA has been considered as a potential hydrogen storage material [3,4]. FA can decompose through either dehydrogenation/decarboxylation ($\text{HCO}_2\text{H} \rightarrow \text{CO}_2 + \text{H}_2$) or dehydration/decarbonylation ($\text{HCO}_2\text{H} \rightarrow \text{CO} + \text{H}_2\text{O}$) [5]. However, for the fuel cell applications, the latter one is an undesirable reaction due to the toxic effect of carbon monoxide on the fuel cell catalysts [6]. Therefore, efficient catalysts are required to selectively promote FA dehydrogenation rather than dehydration.

Platinum [7], gold [8], and palladium [9] are well known heterogeneous catalysts used in decomposition of FA. Much attention has been paid to the palladium catalysts for the dehydrogenation of FA due to the high cost of platinum and gold. Although there exist limited reports on the monometallic palladium nanoparticles used as catalysts in dehydrogenation of FA [10,11], various palladium

based bimetallic and trimetallic catalysts including Ag-Pd [12], Au-Pd [5,13], and AgAu-Pd [14], Pd-Au-Dy [15], CoAgPd [16] have been developed for this reaction. These multimetallic nanoparticles of palladium have been deposited on different supports such as carbon black [17], graphene [18,19], MSC-30 [20], MOFs [5], SBA-15 [21]. A close inspection of the results of studies on different oxide supports reveals that dehydration of FA is favored on acidic oxides while dehydrogenation of FA occurs on basic oxides [22]. Therefore, we consider the basic oxide ceria [23] as promising support for dehydrogenation of FA. The use of ceria as support has been reported in many reactions such as oxidation of organic compounds [24], hydrogenation of aromatics [25], decomposition of nitrous oxide and acetic acid [26,27], soot combustion [28,29], decomposition of formic acid [30,31], water-gas shift reactions [32,33], hydrogen generation from ammonia borane [34–37] and hydrazine borane [38]. CeO_2 has attracted much attention as catalyst support because of its redox properties arising from similar energy of the 4f and 5d levels and low potential energy barrier to electron density distribution between them [39]. Cerium oxides have cerium(III) defects which can readily be formed because of the favorable large positive standard reduction potential of $\text{Ce}^{4+} \rightarrow \text{Ce}^{3+}$ (1.76 V in acidic solution) [40]. Formation of cerium(III) causes an excess negative charge to build up on the oxide surface which enhances

* Corresponding author.

E-mail address: sozkar@metu.edu.tr (S. Özkar).

the coordination of metal(0) nanoparticles to the oxide surface [41]. The valence and defect structure of CeO_2 may change spontaneously because of the doping with other ions [42,43]. Therefore, the high catalytic activity of metal nanoparticles supported on ceria is closely linked to how easily the cerium can change its oxidation state under the conditions [44].

Herein we report that ceria supported monometallic palladium(0) nanoparticles (Pd^0/CeO_2) are highly effective catalysts in releasing CO -free H_2 from FA at room temperature. For comparison palladium nanoparticles were supported on the following oxides with the average particle size given in parentheses: ceria (CeO_2 , 25 nm), silica (SiO_2 , 12 nm), alumina (Al_2O_3 , 13 nm), titania (TiO_2 , 25 nm), zirconia (ZrO_2 , 100 nm), and hafnia (HfO_2 , 100 nm). This comparative study shows that Pd^0/CeO_2 has superior catalytic activity with a turnover frequency of $\text{TOF} = 1400 \text{ h}^{-1}$ in hydrogen generation from FA at $25.0 \pm 0.1^\circ\text{C}$.

2. Experimental

2.1. Materials

Palladium(II) nitrate hydrate ($\text{Pd}(\text{NO}_3)_2 \cdot x\text{H}_2\text{O}$), nanoceria (CeO_2 , particle size ≈ 25 nm; BET surface area is $48.1 \text{ m}^2/\text{g}$), nanozirconia (ZrO_2 , particle size ≈ 100 nm), nanoalumina (Al_2O_3 , particle size ≈ 13 nm), nanosilica (SiO_2 , particle size ≈ 12 nm), nanotitania (TiO_2 , particle size ≈ 25 nm), hafnia (HfO_2 , particle size ≈ 100 nm), formic acid (HCOOH , >95%) sodium borohydride (NaBH_4 , 98%) and sodium formate (HCOONa , >99%) were purchased from Aldrich. Soda lime, containing $\text{Ca}(\text{OH})_2$ (75%), NaOH (3%), KOH (1%) and H_2O (20%), was used as carbon dioxide trap. Distilled water was used in all experiments. All glassware and Teflon-coated magnetic stir bars were cleaned with acetone, followed by copious rinsing with distilled water before drying in an oven at 150°C .

2.2. Characterization

The palladium contents of the Pd^0/CeO_2 samples were determined by Inductively Coupled Plasma Optical Emission Spectroscopy (ICP-OES, Leeman-Direct Reading Echelle) after each sample was completely dissolved in the mixture of HNO_3/HCl (1/3 ratio). high resolution transmission electron microscopy (HRTEM), high angle annular dark-field scanning transmission electron microscopy (HAADF-STEM), and element analysis mapping and energy dispersive X-ray spectroscopy (EDX) were performed on FEI Tecnai G2 F30 transmission electron microscope (TEM) to analyse the microstructure of palladium nanoparticles on ceria. The X-ray photoelectron spectroscopy (XPS) analysis was performed on a Physical Electronics 5800 spectrometer equipped with a hemispherical analyzer and using monochromatic $\text{Al K}\alpha$ radiation of 1486.6 eV, the X-ray tube working at 15 kV, 350 W and pass energy of 23.5 keV.

The evolved gas was analyzed by an equipment having four different sensors: CO detector (Gascard NG/Edinburg Instruments, 0–3% CO, detection limit 10 ppm), CO_2 detector (Gascard NG/Edinburg Instruments, 0–10% CO_2 , detection limit 0.01%), O_2 detector (Model 3290/Teledyne Analytical Instruments, 0–21% O_2), and H_2 detector (Model 2000 XTC/Teledyne Analytical Instruments, 0–5% H_2). No carbon monoxide was detected in evolved gases.

2.3. Preparation of palladium(0) nanoparticles supported on ceria

Ceria (500 mg) was added to a solution of $\text{Pd}(\text{NO}_3)_2 \cdot x\text{H}_2\text{O}$ (in the amount required for the desired palladium loading) in 100 mL H_2O in a 250 mL round bottom flask. This slurry was stirred at room temperature for 18 h than NaBH_4 (50 mM in 10 mL H_2O) solution was added dropwise. After 1 h stirring Pd^0/CeO_2 were formed

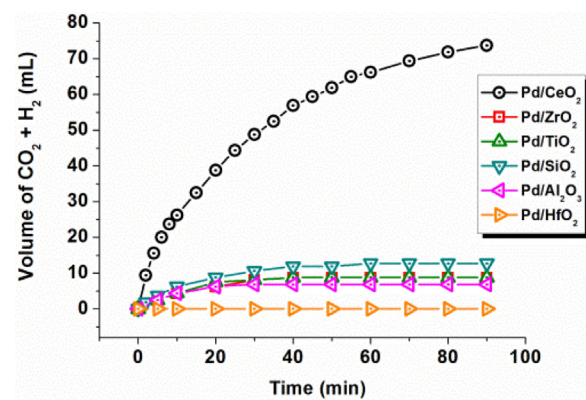


Fig. 1. The plots of generated gas ($\text{CO}_2 + \text{H}_2$) versus time for the dehydrogenation of FA at $25.0 \pm 0.1^\circ\text{C}$ using palladium nanoparticles supported on various oxides. For each tests, Pd concentrations and SF/FA molar ratio were kept constant as 1.6 mM and SF/FA = 9:1, respectively.

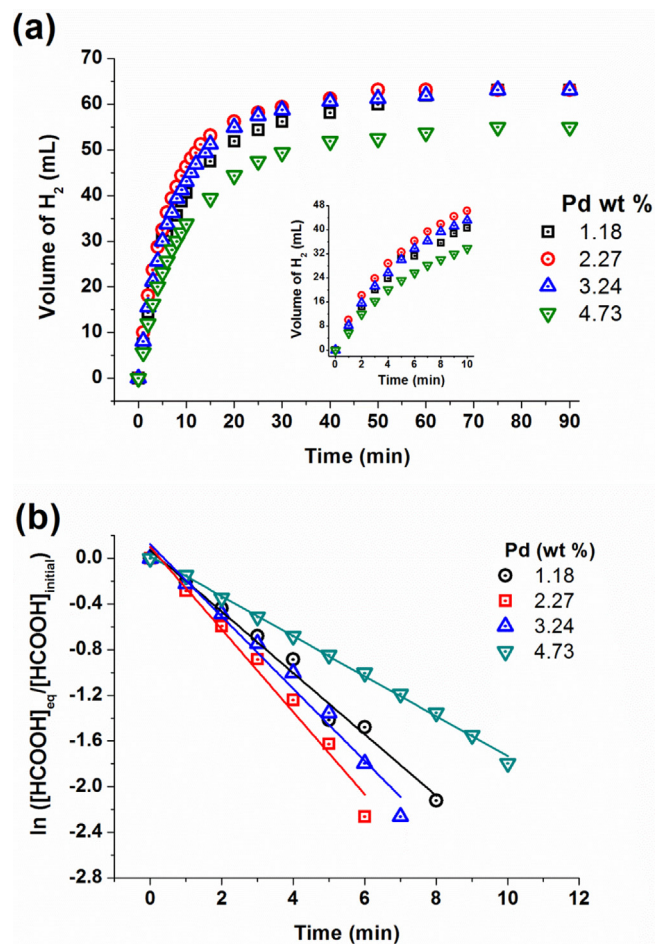


Fig. 2. (a) Hydrogen evolution from the aqueous solution of SF and FA at the molar ratio of SF/FA = 9:1 at $25.0 \pm 0.1^\circ\text{C}$ using Pd^0/CeO_2 catalysts with different palladium loadings. Pd concentrations are kept constant as 1.6 mM Pd (The inset shows enlarged graph in 10 min). (b) $\ln([\text{FA}]_{\text{eq}}/[\text{FA}]_{\text{initial}})$ versus time plot in the first 10 min of dehydrogenation indicating that the reaction is first order with respect to the formic acid concentration.

and the sample was isolated by centrifugation and washed with 250 mL of distilled water and the remnant was dried under vacuum (10^{-3} Torr) at 60°C for 12 h. For comparison, Pd^0/ZrO_2 , Pd^0/SiO_2 , $\text{Pd}^0/\text{Al}_2\text{O}_3$, Pd^0/TiO_2 and Pd^0/HfO_2 were prepared by following the

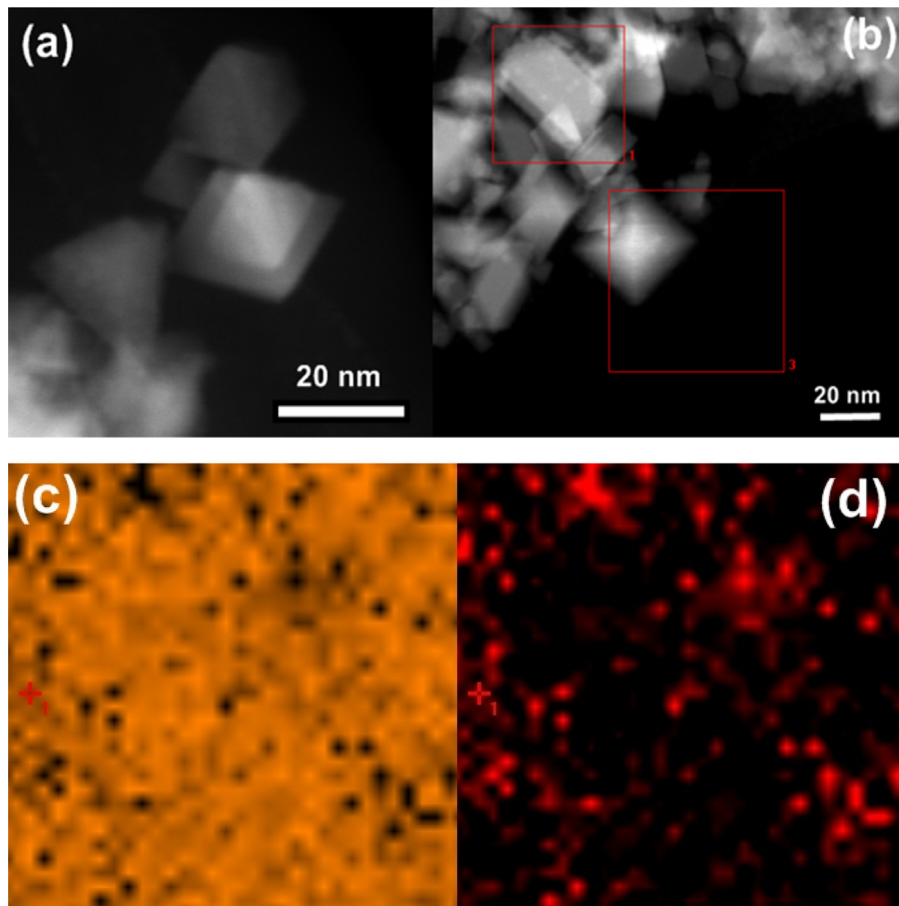


Fig. 3. a) STEM image of CeO₂ (for comparison) and b) STEM image of Pd⁰/CeO₂ (2.27% wt. Pd) at scale bar of 20 nm and STEM –EDX mapping of c) Ce (yellow) and d) Pd (red) taken from the marked area 1 in figure b. (For interpretation of the references to colour in this figure legend, the reader is referred to the web version of this article.)

same procedure as described above, by using zirconia, silica, alumina, titania and hafnia, respectively instead of ceria.

2.4. Dehydrogenation of formic acid using Pd⁰/CeO₂

Before starting the dehydrogenation of FA, a jacketed reaction flask (20 mL) containing a Teflon-coated stir bar was placed on a magnetic stirrer (Heidolph MR-301) and thermostated to 25.0 ± 0.1 °C by circulating water through its jacket from a constant temperature bath. Then, a graduated glass tube (60 cm in height and 3.0 cm in diameter) filled with water was connected to the reaction flask to measure the volume of the gas to be evolved from the reaction. The oxygen in experimental set up (see Fig. S1) was removed by N₂ filling and purging. Next, desired amount of Pd⁰/CeO₂ was dispersed in 10 mL distilled water in the reaction flask thermostated at 25.0 ± 0.1 °C. Then, 0.06 mL formic acid (FA) and 918 mg sodium formate (SF) (the molar ratio of FA/SF = 1/9) was added into the flask containing 9.4 mL of distilled water and the reaction medium was stirred at 1200 rpm. All reactions, unless otherwise stated, were performed under steady magnetic stirring (1200 rpm) at 25.0 ± 0.1 °C. The evolved volume of gas was measured by recording the displacement of water level every 2 min at constant atmospheric pressure of 0.91 atm. The evolved gas was qualitatively analyzed and no carbon monoxide evolution was observed. The catalytic activity of Pd⁰/ZrO₂, Pd⁰/SiO₂, Pd⁰/Al₂O₃, Pd⁰/TiO₂ and Pd⁰/HfO₂ were also tested by following the same procedure as described above under the same conditions at the same palladium concentrations.

2.5. Determination of the most active palladium loading for Pd⁰/CeO₂ used in dehydrogenation of formic acid

The catalytic activity of Pd⁰/CeO₂ samples with various palladium loading in the range of 1.0–5.0% wt. was tested in dehydrogenation of formic acid starting with 1.6 mM Pd and aqueous solution of FA/SF (1:9) in 10 mL of water at 25.0 ± 0.1 °C.

2.6. Testing the reusability of Pd⁰/CeO₂ in dehydrogenation of formic acid

After the complete dehydrogenation of formic acid starting with 3.2 mM Pd and aqueous solution of FA/SF (1:9) in 10 mL of water at 25.0 ± 0.1 °C, the catalyst was isolated as dark grey powder by centrifugation and dried under vacuum (10⁻³ Torr) at 60 °C after washing with 50 mL of water. The isolated samples of Pd⁰/CeO₂ were weighed and redispersed in aqueous solution of FA/SF (1:9) in 10 mL of water for a subsequent run of hydrolysis at 25.0 ± 0.1 °C.

3. Results and discussion

A series of survey experiments were performed to find out the best support for the palladium(0) nanoparticles which would provide the highest catalytic activity in dehydrogenation of formic acid at room temperature. First, palladium(II) ions were impregnated from the aqueous solution of palladium(II) nitrate on one of the following supports: CeO₂, SiO₂, Al₂O₃, TiO₂, ZrO₂ and HfO₂. Then, the impregnated palladium(II) ions were reduced by sodium borohydride at room temperature yielding Pd⁰/CeO₂, Pd⁰/SiO₂, Pd⁰/Al₂O₃,

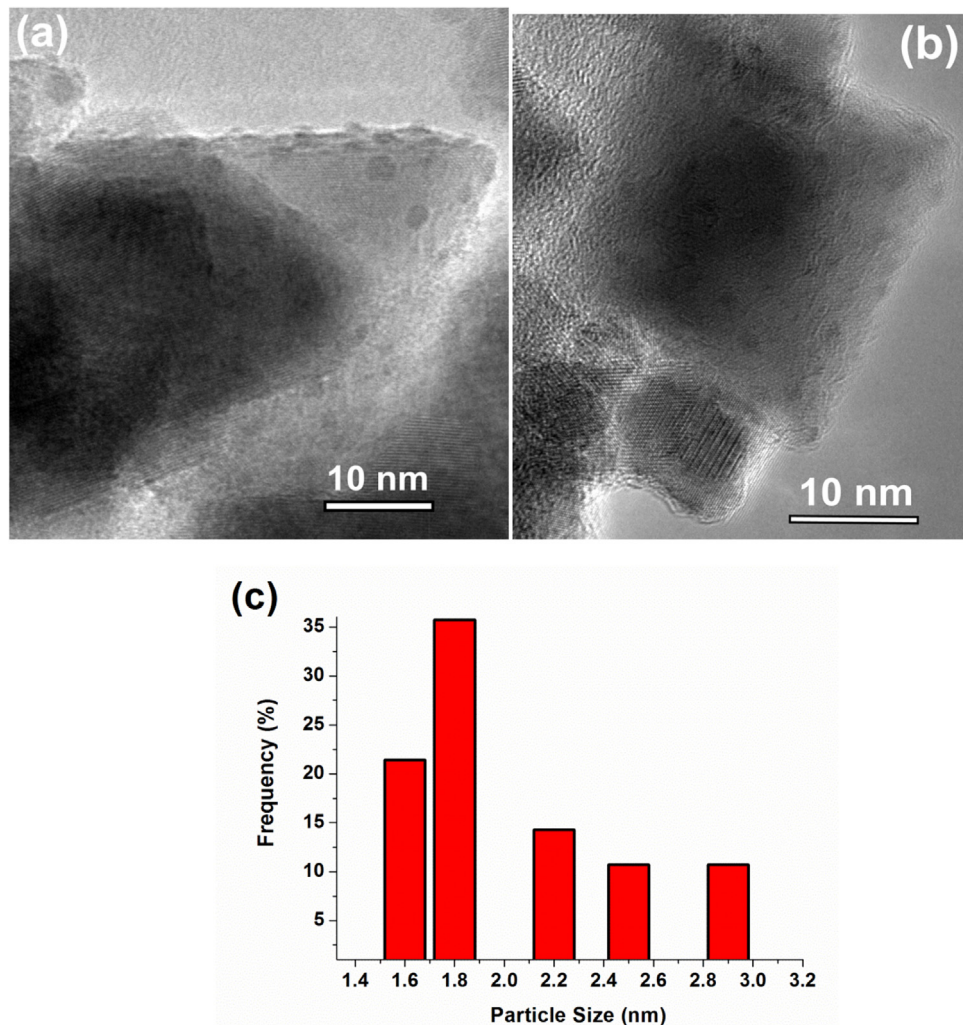


Fig. 4. TEM images of Pd^0/CeO_2 (2.27% wt.Pd) (a-b) and the corresponding histogram showing the particle size distribution (c).

Pd^0/TiO_2 , Pd^0/ZrO_2 and Pd^0/HfO_2 respectively. The metal content of the isolated powders was determined by inductively coupled plasma atomic emission spectroscopy (ICP-OES). The supported palladium(0) nanoparticles were tested in dehydrogenation of formic acid. Fig. 1 shows volume of generated gas ($\text{CO}_2 + \text{H}_2$) versus time plots for the dehydrogenation of formic acid starting with palladium(0) nanoparticles on different oxide supports: Pd^0/CeO_2 (3.24% wt. Pd), Pd^0/SiO_2 (3.05% wt. Pd), $\text{Pd}^0/\text{Al}_2\text{O}_3$ (3.13% wt. Pd), Pd^0/TiO_2 (3.10% wt. Pd), Pd^0/ZrO_2 (3.30% wt. Pd) and Pd^0/HfO_2 (3.0% wt. Pd) all in 1.6 mM Pd concentration at 25 °C. Among the catalysts tested, palladium(0) nanoparticles supported on nanoceria show the highest catalytic activity in dehydrogenation of formic acid at room temperature. Therefore, we decided to use nanoceria as support for the further investigation on palladium(0) nanoparticles catalysts in dehydrogenation of formic acid. The unique performance of the Pd^0/CeO_2 in dehydrogenation of FA can be attributed to both the active component palladium and the combination of palladium nanoparticles with cerium oxide support.

The catalytic activity of Pd^0/CeO_2 in dehydrogenation of FA at 25.0 ± 0.1 °C shows dependence on the Pd loading of ceria as seen from the H_2 volume versus time plots in Fig. 2a. All the plots in Fig. 2a were obtained by collecting the pure H_2 gas after a carbon dioxide trap. Hence, turnover frequency (TOF) for the H_2 generation from FA could be calculated from the initial rate measured in each plot (Fig. 2a). TOF values are found to be 1050, 1400, 1140, and 788 h^{-1} for the 1.18, 2.27, 3.24, and 4.73% wt Pd loaded ceria,

respectively. Since the Pd^0/CeO_2 catalyst with Pd loading of 2.27% wt provides the highest catalytic activity in dehydrogenation of FA it was used in all characterizations performed in this study.

The presence of highly dispersed palladium nanoparticles on the surface of nanoceria was confirmed by scanning tunneling microscope-energy dispersive X-ray spectroscopy (STEM-EDX) and STEM mapping of Pd nanoparticles which were taken from several parts of Pd^0/CeO_2 at different scale (Figs. 3 and S2).

Transmission electron microscopy (TEM) images of Pd^0/CeO_2 (2.27% wt. Pd) in Fig. 4 show the presence of palladium nanoparticles on the surface of nanoceria with a particle size in the range 1.6–4.0 nm (mean diameter: 1.9 ± 0.4). Pd^0/CeO_2 (4.73% wt. Pd) has a mean diameter of 2.5 ± 0.6 nm (Fig. S3). The larger particle size could be the reason for the lower catalytic activity of Pd^0/CeO_2 (4.73% wt. Pd) than that of Pd^0/CeO_2 (2.27% wt. Pd) in dehydrogenation of FA.

XRD patterns of CeO_2 and Pd^0/CeO_2 at different Pd loading (Fig. 5) give peaks at 28.5° , 33.07° , 47.08° , 56.33° and 59.08° assigned to the (111), (200), (220), (311) and (222) reflections of CeO_2 , respectively (JPDF = 43-1002). There is no observable change in the position of the characteristic diffraction peaks of ceria, indicating that ceria framework remains intact after palladium loading. There is no observable peak attributable to palladium nanoparticles in Fig. 5, most likely as a result of low palladium loading on ceria.

X-ray photoelectron spectroscopy (XPS) is used to analyze the chemical state of Pd and Ce on Pd^0/CeO_2 nanopowder. The XPS scan

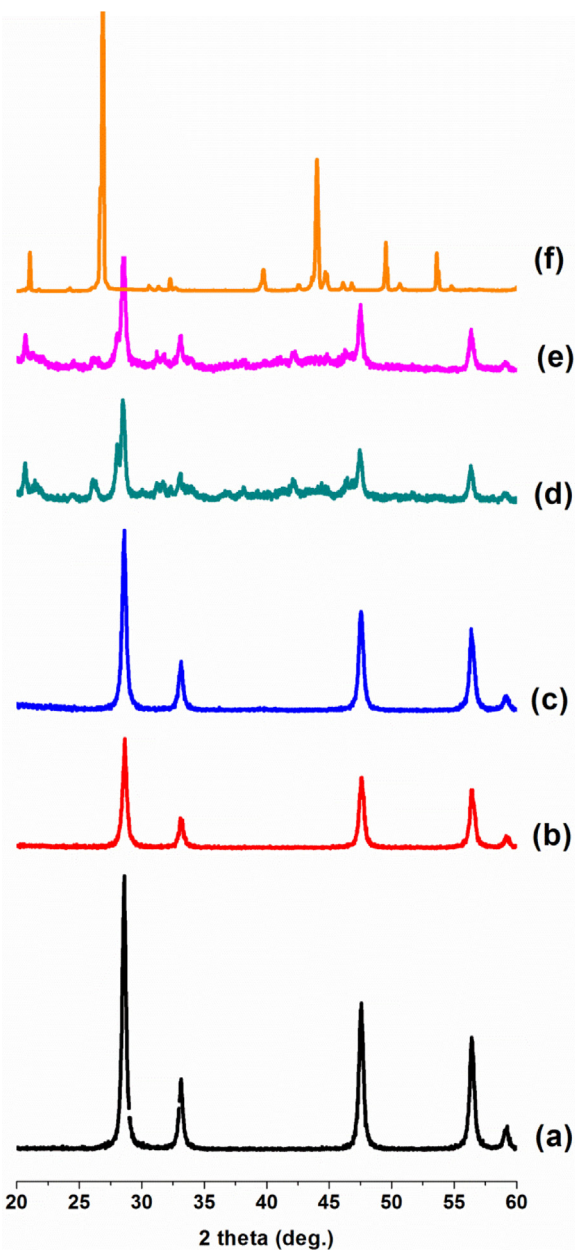


Fig. 5. XRD pattern of a) CeO_2 , b) Pd^0/CeO_2 (2.27% wt Pd), c) Pd^0/CeO_2 (4.73% wt Pd), d) Pd^0/CeO_2 (2.27% wt Pd) after reuse test, e) Pd^0/CeO_2 (4.73% wt Pd) after reaction, f) pure sodium formate.

of Pd 3d (Fig. 6a) shows two prominent bands at 340.6 and 335.3 eV which can readily be assigned to $\text{Pd}(0)$ $3d_{3/2}$ and $3d_{5/2}$, respectively, by comparing to the values of metallic palladium [45,46]. The low intensity bands at 342.1 and 336.5 eV are attributable to palladium oxide [47,48], which might be formed during the XPS sampling. The electronic and surface change in cerium ions in ceria framework after palladium loading was also identified by XPS analysis (Fig. 6b–c). Since the Ce 4d spectra are not surface sensitive (Fig. 6c), XPS spectra of Ce 3d for CeO_2 and Pd^0/CeO_2 (2.27% wt Pd) (Fig. 6b) were analyzed to estimate the extend of cerium reduction. The results reveal that cerium exists dominantly in oxidation state of +4 in the Pd^0/CeO_2 ($\text{BE} = 914.0, 904.3, 900.6, 898.6, 896.2, 886.5, 882.6$, and 880.17 eV) with a small amount of Ce^{3+} (the satellite peaks shown in dark blue at $900.6, 897.1, 884.3$, and 878.2 eV) (Fig. 6b). From the ratio of the total integrated areas of the Gaussian fitting peaks for the Ce^{3+} and Ce^{4+} states [49,50], the percentage of

Ce^{3+} present in the Pd^0/CeO_2 (2.27% wt. Pd) could be estimated to be 3.8%.

Fig. 7 shows the plots of gas volume versus time for the dehydrogenation of formic acid with various molar ratios of SF/FA using Pd^0/CeO_2 (2.27% wt. Pd) catalyst at 25.0 ± 0.1 °C. In all of the tests no carbon monoxide was detected in the collected gas (Fig. S4), indicating that Pd^0/CeO_2 selectively promote the dehydrogenation over the dehydration of FA. When no SF is added to the solution, dehydrogenation of FA is slow releasing only 27 mL of gas at room temperature in 1 h. The highest catalytic activity of Pd^0/CeO_2 is observed when the molar ratio of SF/FA is 9:1. It is noteworthy that 9.3 mL of gas is released when the molar ratio of SF/FA is 9:0, i.e. without the addition of FA at room temperature. This observation indicates the involvement of formate ion in the dehydrogenation (vide infra). Parallel to the increase in SF/FA ratio, one observes an increase in pH of the reaction solution before and after the catalytic reaction (the legend in Fig. 7) and in the catalytic activity of Pd^0/CeO_2 in dehydrogenation of FA [51].

Inspection of plots in Fig. 7 reveals two striking features of hydrogen evolution from the aqueous solution of formic acid and sodium formate at various molar ratios in the presence of Pd^0/CeO_2 (2.27% wt): i) H_2 evolution is also observed from the solution of SF without added FA (at molar ratio SF/FA = 9:0), ii) the amount of H_2 gas collected from the dehydrogenation of FA + SF solution is greater than 1 equivalent per mole of FA added to the solution at the beginning [52]. This has been misinterpreted in literature by considering dehydrogenation of SF through the hydrogen carbonate ion [53,54]. In addition to the dehydrogenation of formic acid (Eq. (1)), one has to consider the ionization of formic acid yielding the conjugate base formate ion (Eq. (2)). Thus, the formate ion and FA exist in reaction medium at equilibrium. The consideration of Eq. (2) enables us to establish the kinetics of dehydrogenation. As the formic acid undergoes dehydrogenation (Eq. (1)) the equilibrium shifts to the left by generating more formic acid from the hydrolysis of formate ion (Eq. (2)). The equilibrium constant is expressed in Eq. (3) where x is the concentration of $[\text{H}_3\text{O}^+]$ or the concentration of formic acid dissociated, and $K_a = 1.80 \times 10^{-4}$ at 298 K [55]. As the dehydrogenation of formic acid produces 1 equivalent H_2 , the equilibrium concentration of FA can be calculated from the H_2 data (Eq. S4 derived from Eq. (3)).



$$K_a = \frac{[\text{HCOO}^-][\text{H}_3\text{O}^+]}{[\text{HCOOH}]} = \frac{(x + [\text{HCOO}^-]_{\text{initial}})x}{[\text{HCOOH}]_{\text{initial}} - [\text{HCOOH}]_{\text{reacted}} - x} \quad (3)$$

Fig. 8b shows the change in equilibrium concentration of formic acid $[\text{FA}]_{\text{eq}}$ in the course of reaction. As the dehydrogenation of FA is first order with respect to FA (Fig. 2b), the reaction becomes very slow when the FA concentration is low after 7 min. Note that when SF is present in large amount, the FA concentration does not get zero because of hydrolysis of SF and the dehydrogenation of FA also continues tough very slowly. As clearly seen from the gas evolutions from aqueous solution of SF (without FA) and FA (without SF) in Fig. 7, the equilibrium between FA and formate ion plays a crucial role in generating H_2 from FA. Although sodium formate has erroneously been considered as an additive for the dehydrogenation of FA in literature [56], we demonstrate that it is converted to formic acid and, thus, indirectly generates H_2 through the dehydrogenation of formic acid.

Comparison of TOF values reported for the most active catalysts in dehydrogenation of FA (Fig. 9) shows that Pd^0/CeO_2 with 2.27% wt Pd loading provides superb catalytic activity ($\text{TOF} = 1400 \text{ h}^{-1}$) in dehydrogenation of FA at 25.0 ± 0.1 °C (See Fig. S5 for the TOF values at different temperatures). It is noteworthy that most of the

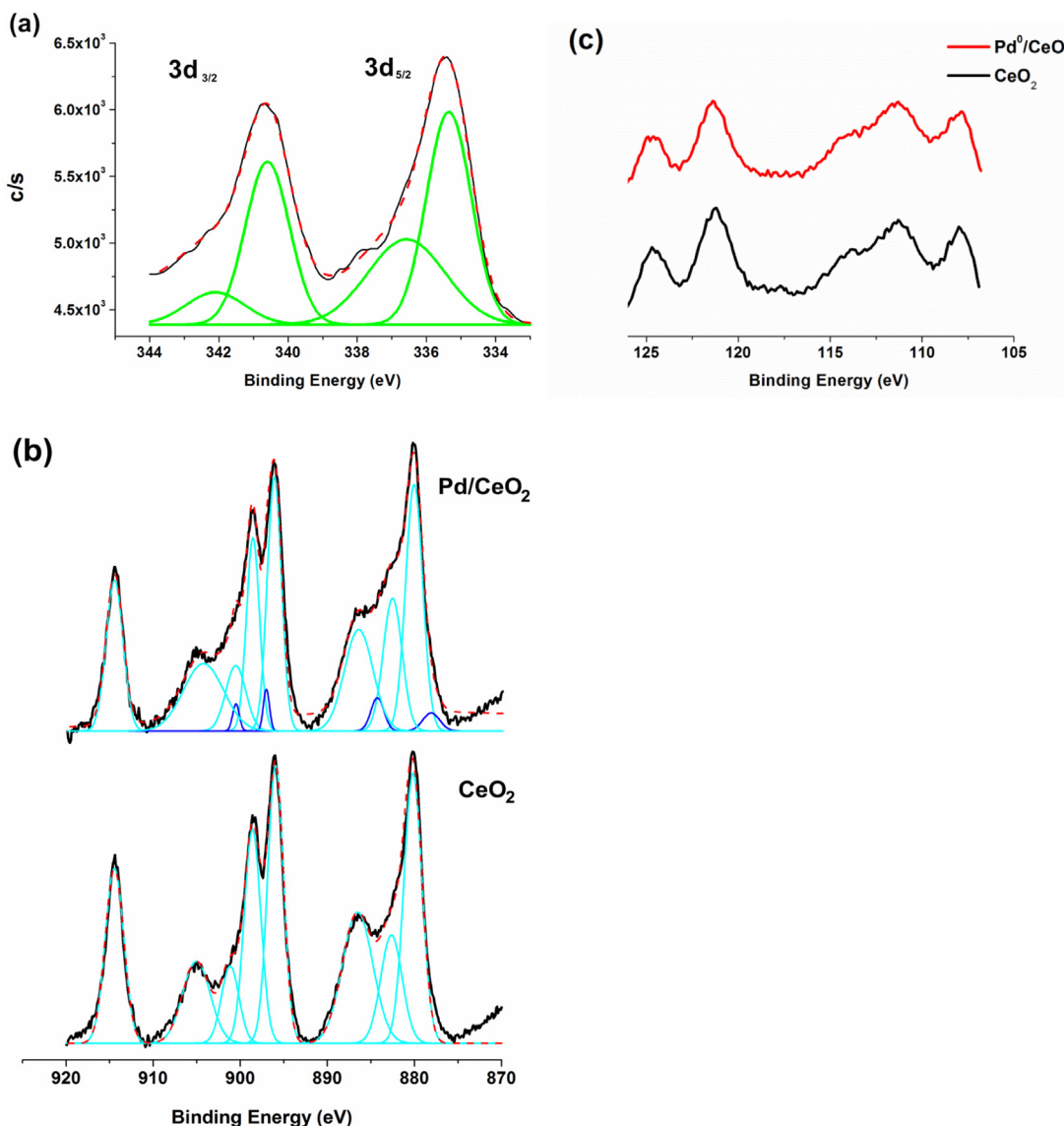


Fig. 6. a) The XPS scan and deconvolution of Pd 3d bands of Pd^0/CeO_2 (2.27% wt.Pd), b) XPS scan and deconvolution of Ce 3d bands of CeO_2 and Pd^0/CeO_2 , c) XPS scan of Ce 4d bands in CeO_2 and Pd^0/CeO_2 .

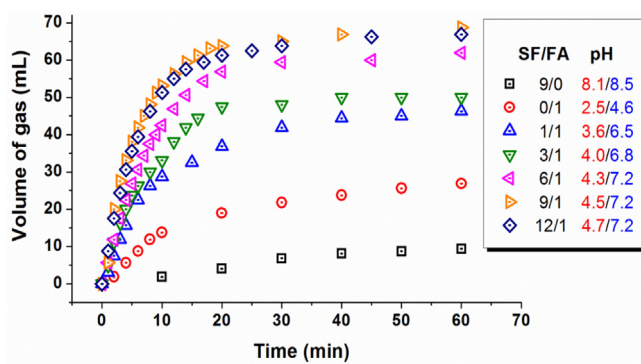


Fig. 7. The plots of generated gas ($\text{CO}_2 + \text{H}_2$) versus time for the dehydrogenation of FA at different molar ratio of SF and FA catalyzed by Pd^0/CeO_2 (2.27% wt. Pd) at room temperature. The pH values of the reaction solution measured before/after catalytic dehydrogenation are given in the legend.

reported catalysts (Table 1) include bimetallic/trimetallic nanoparticles with special functional groups or doping agents. Pd^0/CeO_2 ,

prepared without any pre-treatment by acid-base or any other additives is a unique monometallic catalyst evolving CO free H_2 from dehydrogenation of FA at 298 K with a TOF value of 1400 h^{-1} . It is also noteworthy that the support does have significant effect on the catalytic properties. However, there is no clear insight explaining the high activity of the catalysts according to the type of supporting material and the particle size of metal nanoparticles (Table 1).

Cerium oxides contain cerium(III) defects which can readily be formed because of the favorable large positive standard reduction potential of $\text{Ce}^{4+} \rightarrow \text{Ce}^{3+}$ (1.76 V in acidic solution) [40]. It is conceivable that the interconversion of two oxidation states cerium(IV) and cerium(III) can occur under the catalytic reaction conditions, that is, ceria can undergo redox cycling in aqueous solution [72]. In photocatalytic hydrogen generation from ammonia borane using chromium based amine-functionalized metal-organic frameworks it has been shown that Ce-doping enhances the catalytic activity and charge separation is promoted by valence fluctuation of $\text{Ce}^{4+}/\text{Ce}^{3+}$ under the catalytic conditions [73]. To understand whether Ce^{3+} ions are responsible for the high activity in formic acid decomposition, solution of Ce^{3+} ions externally prepared by

Table 1

Catalytic activity of various catalysts in dehydrogenation of FA (TOF values were taken directly from the related studies).

Catalyst	FA/SF (mmol/mmol)	Temp. (K)	n _{metal} (mmol)	TOF _{initial} (mol gas.mol metal. ⁻¹ h ⁻¹)	Average particle size (nm)	Ref.
Ag ₄₂ Pd ₅₈ /C	10/0	323	0.032	382 ^a	2.2	[57]
Au ₄₁ Pd ₅₉ /C	10/0	323	0.190	230 ^a	4.0	[58]
AuPd-CeO ₂ /N-rGO	5/0	298	0.100	52.9	3.3	[59]
Colloidal Pd-poly(allyl-amine)	15.2/0	295	0.040	37.8	2.5	[60]
CoAuPd/C	5/0	298	0.100	80 ^a	20	[61]
PtRuBiOx/C	318/0	353	0.0013	312 ^a	5.0	[62]
Ag@Pd core-shell NPs	10/0	293	0.200	125 ^a	–	[12]
B-doped Pd/C	11/8	303	0.047	1184 ^a	4.1	[54]
Au ₈ Pd ₄ /C	11/40	298	0.017	1075 ^a	2.0	[63]
Pd ⁰ /CeO ₂ (2.27% wt.Pd)	1.5/13.4	298	0.016	1400	1.9	This Study
Pd ⁰ /CeO ₂ (2.27% wt.Pd)	1.5/13.4	303	0.016	2040	1.9	This Study
NaOH assisted-Pd/MSC-30	9/9	298	0.09	750	2.3	[20]
Pd-S-SiO ₂	36/4	358	0.03	719 ^a	–	[11]
Ag ₁₈ Pd ₈₂ @ZIF-8	3/1	353	0.094	580 ^a	1.6	[64]
PdNi@Pd/GNs-CB	5/5	298	0.20	577	–	[65]
Pd/C—NaBH ₄	11/8	303	0.047	304 ^a	2.2	[54]
PdAu/ED-MIL-101	3.04/1.02	363	0.026	106	2.0–8.0	[5]
Pd-NH ₂ /MIL-125	9.8/7.9	305	0.0023	214	3.1	[66]
Citric acid modified Pd/C	5.3/4.2	298	0.047	64	2.8	[67]
PdAu/C-CeO ₂	49.7/16.65	365	0.113	113	2.0–4.0	[68]
Ag _{0.1} Pd _{0.9} /rGO	5/3.35	298	0.1	105.2	6.0	[69]
PdAg/C-CeO ₂	49.7/16.65	365	0.113	38	≈8.0	[68]
PdAu@Au/C	33.2/33.2	365	0.227	21.4	16.0	[70]
Methanol mediated Pd NPs/Vulcan XC-72R	9/9	303	0.054	1678	1.4	[71]

^a Denotes the TOF values were calculated according to the amount of released CO₂ + H₂ gases (The remaining TOF values were calculated according to the amount of released H₂ gas).

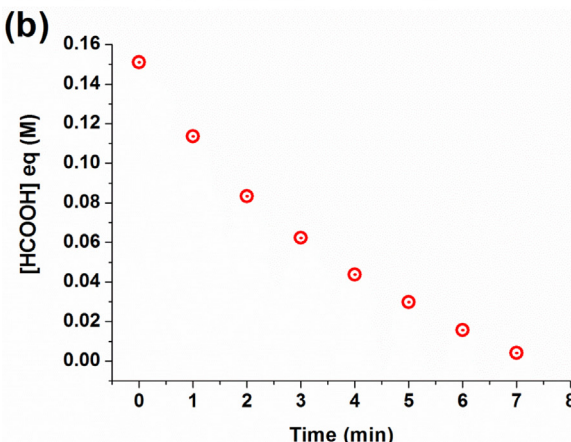
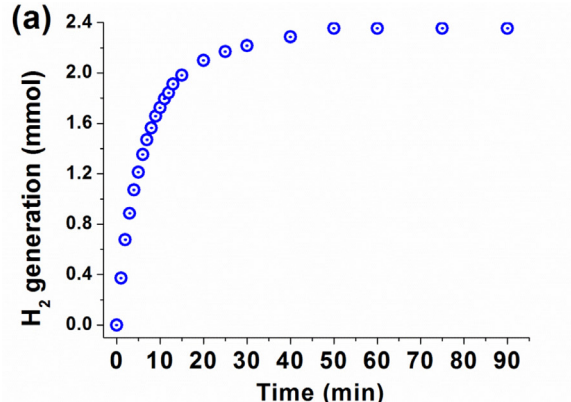


Fig. 8. (a) Hydrogen generation from the aqueous solution of SF and FA at molar ratio of SF/FA=9:1 using Pd⁰/CeO₂ catalysts (2.27% wt. Pd) at 25.0±0.1°C, (b) the corresponding change in formic acid concentration during the dehydrogenation.

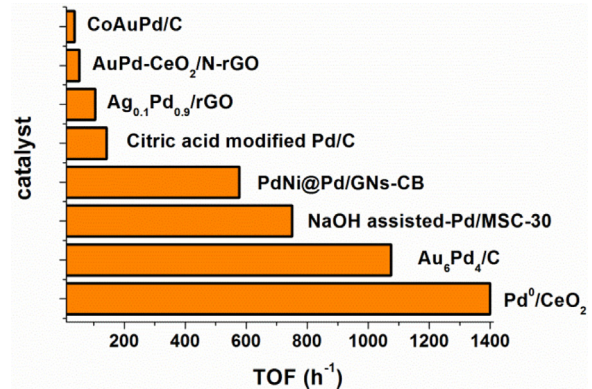


Fig. 9. Comparison of TOF values of reported catalysts used in dehydrogenation of formic acid at 298 K.

dissolving Ce(NO₃)₃ at different concentrations was added into the reaction medium. As shown in Fig. 10, the addition of the Ce³⁺ ions did not alter significantly the catalytic activity of Pd⁰/CeO₂ in dehydrogenation of formic acid at room temperature. Ce³⁺ doped Pd⁰/CeO₂ catalyst was also prepared (see SI) and tested in dehydrogenation of formic acid to observe the effect of added Ce³⁺ ions on the surface of the catalyst. However no improvement was achieved in the catalytic activity of Pd⁰/CeO₂ in dehydrogenation of formic acid (Fig. S7). Nevertheless XPS analysis (Fig. 6) provides evidence for the existence of Ce³⁺ ion in Pd⁰/CeO₂ supporting the hypothesis that the recycling of Ce⁴⁺/Ce³⁺ under the catalytic conditions is responsible for the catalytic enhancement of palladium nanoparticles.

Reusability of Pd⁰/CeO₂ (2.27% wt. Pd) catalyst was tested in successive runs of dehydrogenation of FA at room temperature. The results of reusability tests reveal that Pd⁰/CeO₂ does provide only 50% conversion of FA in the second run (Fig. 11a). The cat-

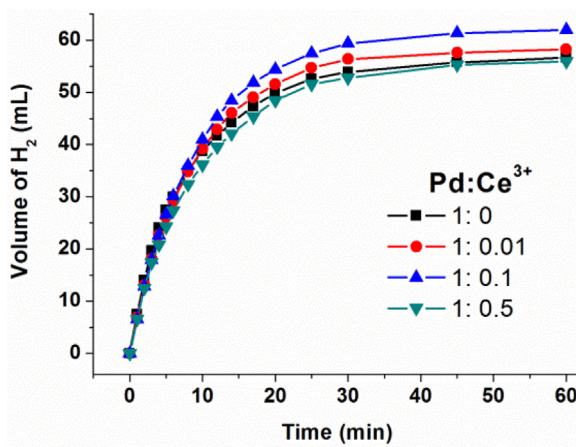


Fig. 10. Hydrogen evolution from the aqueous solution of SF and FA at the molar ratio of SF/FA = 9/1 at room temperature using Pd^0/CeO_2 (2.27% wt.Pd) catalysts (1.6 mM Pd) with aqueous $\text{Ce}(\text{NO}_3)_3$. Ce^{3+} ions were added by changing the mol of $\text{Ce}(\text{NO}_3)_3$ with respect to the mole of palladium on CeO_2 .

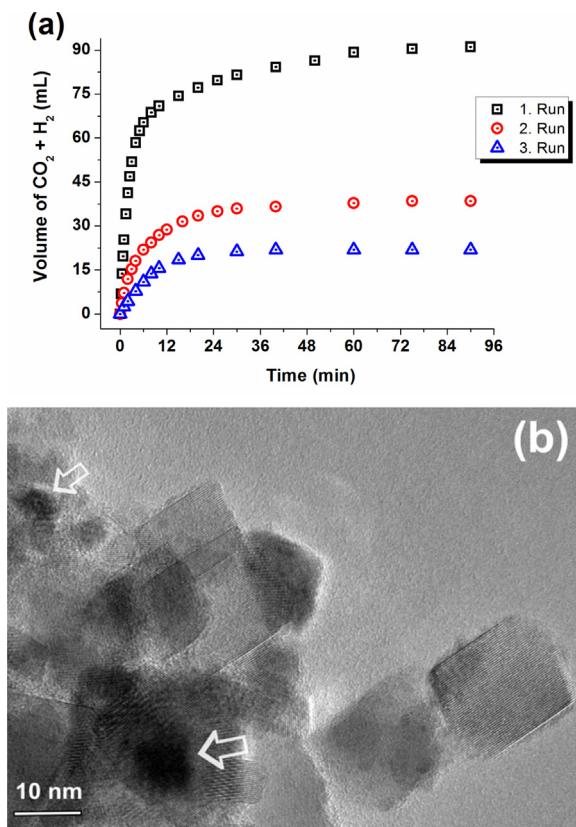


Fig. 11. a) Gas evolution from the aqueous solution of SF and FA at the molar ratio of SF/FA = 9/1 for the first, second and third use of Pd^0/CeO_2 (2.27% wt. Pd) catalysts at $25.0 \pm 0.1^\circ\text{C}$. b) TEM image of Pd^0/CeO_2 sample (2.27% wt. Pd) harvested after the second use in dehydrogenation of FA (palladium nanoparticles indicated with arrow).

alytic activity of the filtrate solution obtained by centrifugation of the solid materials after the second use was tested in the dehydrogenation of FA under the same conditions. The filtrate solution is catalytically silent in dehydrogenation of FA indicating no leaching of palladium into the solution. Therefore, the decrease in catalytic activity after the second run can be attributed to the agglomeration of nanoparticles on the surface of ceria during the isolation, drying and redispersion processes as shown in the TEM image in Fig. 11b for the sample harvested after the second run of dehydro-

genation of FA. The aggregation of palladium nanoparticles on ceria with 4.73% wt Pd loading was also observed after the reaction (Fig. S3c). The XRD patterns of Pd^0/CeO_2 samples at different Pd loadings after the catalytic use and that of pure sodium formate were compared (Fig. 5). Although there is no change in diffraction pattern of ceria nanopowder, the peaks of sodium formate become visible in the XRD pattern of Pd^0/CeO_2 catalysts after the reaction. Therefore, the catalytic activity loss after the reaction can also be attributed to the deposition of sodium formate species on Pd^0/CeO_2 catalysts. Indeed, Pd^0/CeO_2 catalysts show no catalytic activity after the addition of formic acid/sodium formate after the first run, which was performed without isolation, drying and redispersion processes. The deactivation of the catalysts may be attributed to the changes in pH of the reaction medium, the ratio of formic acid/sodium formate and SF residue after the reaction. Therefore, we performed the dehydrogenation of FA using different initial amount of formic acid (the SF/FA ratio was kept constant as 9/1 and required amount of water was added to maintain the same pH for each run) and the total conversion was achieved after each run (Fig. S6).

4. Conclusion

In summary, a highly efficient dehydrogenation of formic acid at room temperature was achieved using palladium(0) nanoparticles supported on nanoceria (Pd^0/CeO_2) as catalysts. Pd^0/CeO_2 with 2.27% wt Pd loading is a superb catalyst for the dehydrogenation of FA with a TOF value of 1400 h^{-1} at room temperature. For the first time, we provided the kinetics of FA dehydrogenation by taking the equilibrium between FA and its conjugate base formate ion into account. Thus the kinetic data, obtained by monitoring the volume of pure H_2 gas, can be converted to the variation in FA concentration. This provides compelling evidence that the dehydrogenation is first order with respect to the FA concentration. Pd^0/CeO_2 were prepared without any pre-treatment by acid-base or any other additives. Therefore, easy preparation, high activity and high selectivity performance of Pd^0/CeO_2 indicate that Pd^0/CeO_2 are promising candidate to be employed in developing highly efficient catalysts in hydrogen generation. This simple facile method developed for the preparation of Pd^0/CeO_2 can be extended to other ceria-based metallic systems in more applications in the field of catalysis.

Acknowledgements

Partial support by Turkish Academy of Sciences (TUBA) is gratefully acknowledged. We would like to thank İlker Yıldız for XPS analyses.

Appendix A. Supplementary data

Supplementary data associated with this article can be found, in the online version, at <http://dx.doi.org/10.1016/j.apcatb.2017.01.063>.

References

- [1] A.K. Singh, S. Singh, A. Kumar, *Catal. Sci. Technol.* 6 (2016) 12–40.
- [2] T.C. Johnson, D.J. Morris, M. Wills, *Chem. Soc. Rev.* 39 (2010) 81–88.
- [3] S. Enthal, *ChemSusChem* 1 (2008) 801–804.
- [4] S. Enthal, J. von Langermann, T. Schmidt, *Energy Environ. Sci.* 3 (2010) 1207–1217.
- [5] X. Gu, Z. Lu, H. Jiang, T. Akita, Q. Xu, *J. Am. Chem. Soc.* 133 (2011) 11822–11825.
- [6] K.V. Kordesch, G.R. Simader, *Chem. Rev.* 95 (1995) 191–207.
- [7] N.M. Markovic, P.N. Ross Jr., *Surf. Sci. Rep.* 45 (2002) 117–229.
- [8] N. Yi, H. Saltsburg, M. Flytzani-Stephanopoulos, *ChemSusChem* 6 (2013) 816–819.
- [9] M. Grasemann, G. Laurenczy, *Energy Environ. Sci.* 5 (2012) 8171–8181.

[10] D.A. Bulushev, S. Beloshapkin, J.R.H. Ross, *Catal. Today* 154 (2010) 7–12.

[11] Y. Zhao, L. Deng, S.Y. Tang, D.M. Lai, B. Liao, Y. Fu, Q.X. Guo, *Energy Fuels* 25 (2011) 3693–3697.

[12] K. Tedsee, T. Li, S. Jones, C.W.A. Chan, K.M.K. Yu, P.a.J. Bagot, E.a. Marquis, G.D.W. Smith, S.C.E. Tsang, *Nat. Nanotechnol.* 6 (2011) 302–307.

[13] W.Y. Yu, G.M. Mullen, D.W. Flaherty, C.B. Mullins, *J. Am. Chem. Soc.* 136 (2014) 11070–11078.

[14] S. Li, Y. Ping, J.-M. Yan, H.-L. Wang, M. Wu, Q. Jiang, *J. Mater Chem A* 3 (2015) 14535–14538.

[15] X. Zhou, Y. Huang, C. Liu, J. Liao, T. Lu, W. Xing, *ChemSusChem* 3 (2010) 1379–1382.

[16] N. Cao, S. Tan, W. Luo, K. Hu, G. Cheng, *Catal. Lett.* 146 (2016) 518–524.

[17] D.A. Bulushev, L.G. Bulusheva, S. Beloshapkin, T. O’Conno, A.V. Okotrub, K.M. Ryan, *ACS Appl. Mater. Interfaces* 7 (2015) 8719–8726.

[18] Z.L. Wang, J.M. Yan, H.-L. Wang, Y. Ping, Q. Jiang, *J. Mater. Chem. A* 1 (2013) 12721–12725.

[19] J.-M. Yan, Z.-L. Wang, L. Gu, S.-J. Li, H.-L. Wang, W.-T. Zheng, Q. Jiang, *Adv. Energy Mater.* 5 (2015) (1500107/1–1500107/6).

[20] Q.-L. Zhu, N. Tsumori, Q. Xu, *Chem. Sci.* 5 (2014) 195–199.

[21] K. Koh, J.E. Seo, J.H. Lee, A. Goswami, C.W. Yoon, T. Asefa, *J. Mater. Chem. A* 2 (2014) 20444–20449.

[22] A. Bandara, J. Kubota, A. Wada, K. Domen, C. Hirose, *J. Phys. Chem. B* 101 (1997) 361–368.

[23] Z. Wu, A.K.P. Mann, M. Li, S.H. Overbury, *J. Phys. Chem. C* 119 (2015) 7340–7350.

[24] S. Hosokawa, Y. Fujinami, H. Kanai, *J. Mol. Catal. A Chem.* 240 (2005) 49–54.

[25] R.S. Suppino, R. Landers, A.J.G. Cobo, *Appl. Catal. A Gen.* 452 (2013) 9–16.

[26] S. Hosokawa, S. Nogawa, M. Taniguchi, K. Utani, H. Kanai, S. Imamura, *Appl. Catal. A Gen.* 288 (2005) 67–73.

[27] S. Hosokawa, H. Kanai, K. Utani, Y.I. Taniguchi, Y. Saito, S. Imamura, *Appl. Catal. B Environ.* 45 (2003) 181–187.

[28] A. Bueno-López, *Appl. Catal. B Environ.* 146 (2014) 1–11.

[29] M. Piumetti, S. Bensaid, N. Russo, D. Fino, *Appl. Catal. B Environ.* 180 (2016) 271–282.

[30] Y. Lykhach, M. Happel, V. Johánek, T. Skála, F. Kollhoff, N. Tsud, F. Dvořák, K.C. Prince, V. Matolín, J. Libuda, *J. Phys. Chem. C* 117 (2013) 12483–12494.

[31] N. Yi, H. Saltsburg, M. Flytzani-Stephanopoulos, *ChemSusChem* 6 (2013) 816–819.

[32] A. Bruijx, J.A. Rodriguez, P.J. Ramírez, S.D. Senanayake, J. Evans, J.B. Park, D. Stacchiola, P. Liu, J. Hrbek, F. Illas, *J. Am. Chem. Soc.* 134 (2012) 8968–8974.

[33] N. Ta, J. Liu, S. Chenna, P.A. Crozier, Y. Li, A. Chen, W. Shen, *J. Am. Chem. Soc.* 134 (2012) 20585–20588.

[34] S. Akbayrak, Y. Tonbul, S. Özkar, *Appl. Catal. B Environ.* 198 (2016) 162–170.

[35] Y. Tonbul, S. Akbayrak, S. Özkar, *Int. J. Hydrogen Energy* 41 (2016) 11154–11162.

[36] S. Akbayrak, Y. Tonbul, S. Özkar, *Dalton Trans.* 45 (2016) 10969–10978.

[37] X. Wang, D. Liu, S. Song, H. Zhang, *Chem. Commun.* 48 (2012) 10207–10209.

[38] Z. Zhang, Z.H. Lu, H. Tan, X. Chen, Q. Yao, *J. Mater. Chem. A* 3 (2015) 23520–23529.

[39] J.P. Holgado, R. Alvarez, G. Munuera, *Appl. Surf. Sci.* 161 (2000) 301–315.

[40] A. Ciftci, S. Eren, D.A.J.M. Ligthart, E.J.M. Hensen, *ChemCatChem* 6 (2014) 1260–1269.

[41] L. He, B. Liang, L. Li, X. Yang, Y. Huang, A. Wang, X. Wang, T. Zhang, *ACS Catal.* 5 (2015) 1623–1628.

[42] G.S. Herman, *Surf. Sci.* 437 (1999) 207–214.

[43] E. Mamontov, T. Egami, V. Pennsyl, R. Brezny, M. Koranne, W.R. Grace, C. Grace, V. Da, S. Tyagi, *J. Phys. Chem. B* 104 (2000) 11110–11116.

[44] C. Sun, H. Li, L. Chen, *Energy Environ. Sci.* 5 (2012) 8475–8505.

[45] D. Briggs, M.P. Seah, *Practical Surface Analysis*, vol. 1, 2nd ed., Wiley, New York, USA, 1990.

[46] A. Tressaud, S. Khairoun, H. Touhara, N.Z. Watanabe, *Anorg. Allg. Chem.* 540–541 (1986) 291–299.

[47] K.S. Kim, a.F. Gossman, N. Winograd, *Anal. Chem.* 46 (1974) 197–200.

[48] W.E. Muddeman, W.C. Bowling, D.C. Carter, D.R. Grove, *Surf. Interface Anal.* 11 (1988) 317–326.

[49] A. Pfau, K.D. Schierbaum, *Surf. Sci.* 321 (1994) 71–80.

[50] T. Naganuma, E. Traversa, *Nanoscale* 4 (2012) 4950–4953.

[51] S. Fukuzumi, T. Kobayashi, T. Suenobu, *J. Am. Chem. Soc.* 132 (2010) 1496–1497.

[52] Q. Lv, L. Feng, C. Hu, C. Liu, W. Xing, H. Wang, Y. Liu, M. Li, H. Huang, H.M. Xu, R.J. Hong, H. Shen, *Catal. Sci. Technol.* 4 (2015) 2581–2584.

[53] X. Wang, G.W. Qi, C.H. Tan, Y.P. Li, J. Guo, X.J. Pang, S.Y. Zhang, *Int. J. Hydrogen Energy* 39 (2014) 837–843.

[54] K. Jiang, K. Xu, S. Zou, W. Bin Cai, *J. Am. Chem. Soc.* 136 (2014) 4861–4864.

[55] P. Atkins, J.D. Paula, *Atkins’ Physical Chemistry*, vol. 8, Oxford University Press, US-Canada, 2006, pp. 1008–1009.

[56] A. Bulut, M. Yurderi, Y. Karatas, Z. Say, H. Kivrak, M. Kaya, M. Gulcan, E. Ozensoy, M. Zahmakiran, *ACS Catal.* 5 (2015) 6099–6110.

[57] S. Zhang, Ö. Metin, D. Su, S. Sun, *Angew. Chem. Int. Ed.* 52 (2013) 3681–3684.

[58] Ö. Metin, X. Sun, S. Sun, *Nanoscale* 5 (2013) 910–912.

[59] Z.-L. Wang, J.-M. Yan, Y.-F. Zhang, Y. Ping, H.-L. Wang, Q. Jiang, *Nanoscale* 6 (2014) 3073–3077.

[60] S. Jones, J. Qu, K. Tedsee, X.Q. Gong, S.C.E. Tsang, *Angew. Chem. Int. Ed.* 51 (2012) 11275–11278.

[61] Z.-L. Wang, J.-M. Yan, Y. Ping, H.-L. Wang, W.T. Zheng, Q. Jiang, *Angew. Chem.–Int. Ed.* 52 (2013) 4406–4409.

[62] S.-W. Ting, S. Cheng, K.-Y. Tsang, N. van der Laak, K.-Y. Chan, *Chem. Commun.* (2009) 7333–7335.

[63] S. Wu, F. Yang, P. Sun, T. Chen, *RSC Adv.* 4 (2014) 44500–44503.

[64] H. Dai, B. Xia, L. Wen, C. Du, J. Su, W. Luo, G. Cheng, *Appl. Catal. B Environ.* 165 (2015) 57–62.

[65] Y. Qin, J. Wang, F. Meng, L. Wang, X. Zhang, *Chem. Commun.* 49 (2013) 10028–10030.

[66] M. Martis, K. Mori, K. Fujiwara, W.S. Ahn, H. Yamashita, *J. Phys. Chem. C* 117 (2013) 22805–22810.

[67] Z.-L. Wang, J.-M. Yan, H.-L. Wang, Y. Ping, Q. Jiang, *Sci. Rep.* 2 (598) (2012) 1–6.

[68] X. Zhou, Y. Huang, W. Xing, C. Liu, J. Liao, T. Lu, *Chem. Commun.* (2008) 3540–3542.

[69] Y. Ping, J.-M. Yan, Z.-L. Wang, H.-L. Wang, Q. Jiang, *J. Mater. Chem. A* 1 (2013) 12188–12191.

[70] Y. Huang, X. Zhou, M. Yin, C. Liuand, W. Xing, *Chem. Mater.* 22 (2010) 5122–5128.

[71] Q.L. Zhu, N. Tsumori, Q. Xu, *J. Am. Chem. Soc.* 137 (2015) 11743–11748.

[72] S.S. Lee, W. Song, M. Cho, H.L. Puppala, P. Nguyen, H. Zhu, L. Segatori, V.L. Colvin, *ACS Nano* 7 (2013) 9693–9703.

[73] M. Wen, Y. Kuwahara, K. Mori, D. Zhang, H. Li, H. Yamashita, *J. Mater. Chem. A* 3 (2015) 14134–14141.